Journal of Physics: Photonics

PAPER

Improvement of optical noise in optical-injection-locked quantum dot lasers epitaxially grown on silicon by reducing external carrier noise

Luochen Qu[1,4], **Qi Chu**[1,4], **Wenlu Wang**[1], **Zhiyong Jin**[1], **Shihao Ding**[2], **Cheng Wang**[3], **Xiaochuan Xu**[1], **Jiawei Wang**[1] **and Jianan Duan**[1,*]

[1] National Key Laboratory of Laser Spatial Information, Guangdong Provincial Key Laboratory of Integrated Photonic-Electronic Chip, School of Integrated Circuits, Harbin Institute of Technology, Shenzhen 518055, People's Republic of China
[2] College of Integrated Circuits and Optoelectronic Chips, Shenzhen Technology University, Shenzhen 518118, People's Republic of China
[3] School of Information Science and Technology, ShanghaiTech University, Shanghai 201210, People's Republic of China
[4] These authors contributed equally to this work.
[*] Author to whom any correspondence should be addressed.

E-mail: duanjianan@hit.edu.cn and wangjw7@hit.edu.cn

Keywords: quantum dot laser, semiconductor laser, spectral linewidth, relative intensity noise

OPEN ACCESS

RECEIVED
13 July 2024

REVISED
28 September 2024

ACCEPTED FOR PUBLICATION
11 October 2024

PUBLISHED
22 October 2024

Abstract

This study theoretically investigates the impact of external carrier noise from pumping sources on the optical noise of epitaxial quantum dot (QD) lasers on silicon. The findings indicate that the spectral linewidth and relative intensity noise (RIN) of silicon-based QD lasers using a quiet pump are significantly reduced. At 5.5 times the threshold current, the spectral linewidth decreases from 337.2 kHz to 213.2 kHz, and the RIN decreases from −141.3 dB Hz^{-1} to −168.8 dB Hz^{-1}. This reduction is attributed to the lower external carrier noise level of the quiet pump, which also suppresses the spectral linewidth rebroadening effect at a high bias current. Moreover, when external optical injection locking is applied, the spectral linewidth further decreases to 24 kHz at an injection ratio of −70 dB and to 1.8 mHz at 0 dB. The RIN also slightly decreases to −172.4 dB Hz^{-1} with an injection ratio of 10. These results demonstrate that using a quiet pump is an effective and manageable strategy for significantly reducing both the spectral linewidth and RIN of QD lasers, thereby facilitating their application in next-generation photonic integrated circuits, continuous-variable quantum key distribution, quantum computing and ultra-precise quantum sensing.

1. Introduction

The emergence and development of quantum communication, optical computing, optical interconnects, and artificial intelligence are driving the further advancement of photonic integrated circuits on silicon, which has become the obvious choice due to its superior optical properties and compatibility with mature complementary metal–oxide–semiconductor technology [1–3]. However, as an indirect bandgap material, silicon has very low light emission efficiency. The traditional III-V materials used for making semiconductor lasers have issues such as lattice mismatch and different polarities with silicon materials, leading to high dislocation densities during the fabrication of silicon-based lasers [4, 5]. This inevitably reduces the light emission efficiency and output quality of the devices, resulting in larger spectral linewidth and relative intensity noise (RIN) [6]. Consequently, the development of on-chip light sources has lagged far behind other silicon-based optical components, becoming a bottleneck for the further development of silicon photonics [1, 7]. In semiconductor lasers, photon fluctuations affect both the intensity and phase of the optical field, resulting in intensity and frequency noise. Quantum well (QW) lasers exhibit spectral linewidths in the MHz range and possess larger RIN, which reduce the signal-to-noise ratio and increase the

bit error rate, thereby posing challenges for applications such as lidar and precision optical measurements. In contrast, the discrete distribution of quantum dot (QD) materials provides several advantages over QW materials. Particularly, QDs are more tolerant to defects in epitaxial growth, effectively deflecting or clamping defects to prevent loop formation, and localizing carriers to inhibit lateral diffusion and non-radiative recombination. This significantly mitigates the impact of dislocation defects on the optical properties of the laser [8, 9]. As a result, silicon-based QD lasers exhibit long lifetimes [10], high thermal stability [11], near-zero linewidth enhancement factors (LEFs) [12], high tolerance to optical feedback [13] and spectral linewidths that can reach the kHz level [14], making them ideal candidates for on-chip light sources [15, 16].

External optical injection locking scheme is an effective technique to further reduce the spectral linewidth and RIN of epitaxial QD lasers on silicon, which can achieve significant linewidth squeezing at very low injection ratios [17]. Moreover, the optical-injection-locked QD lasers exhibit significantly improved dynamic characteristics, such as enhanced modulation bandwidth [18] and reduced frequency chirping [19]. Additionally, optical injection locking is also an effective method for generating photonic microwaves in QD lasers [20, 21]. However, QD lasers with optical injection locking exhibiting excellent linewidth characteristics demand high quality of the injected master laser with narrow linewidth [22]. QD lasers, when used as slave lasers, exhibit spectral linewidth rebroadening [14, 23, 24]. The three-dimensional quantum confinement effect in QDs can lead to discrete energy levels, causing the LEF to increase due to gain compression [23], thermal effects [24], and longitudinal spatial hole burning [14]. These factors contribute to the spectral linewidth rebroadening effect observed at high bias currents in QD lasers. Since optical injection must occur before linewidth rebroadening to effectively reduce the spectral linewidth, this requirement restricts the pumping current range of QD lasers, thereby limiting their applicability [14, 23, 24].

The spectral linewidth and RIN of QD lasers are significantly influenced by external carrier noise. Prior works have demonstrated that controlling external carrier fluctuations can effectively reduce RIN and spectral linewidth [25–27]. This effect is primarily attributed to the distinct electrical pumping mechanism of semiconductor lasers, distinguishing them from other types of lasers. While optical pumping relies on photon absorption governed by a Poisson point process and is constrained by shot noise, electrical pumping in semiconductor lasers, driven by injection currents through a circuit, deviates from a strict Poisson point process due to Coulomb interactions. Consequently, it is feasible to transform a Gaussian distribution of carriers into a sub-Poisson distribution, thereby introducing regularization elements into the electron stream. By reducing the external carrier noise originating from the external pumping sources, a more regularized excitation of atoms is achieved. This regularization subsequently manifests in the photons emitted by these atoms, leading to a reduction in spectral linewidth and RIN [26].

This paper presents a robust and straightforward approach to reducing the spectral linewidth and RIN of silicon-based QD lasers under optical injection locking by mitigating external carrier noise from the pumping source. The investigation includes simulations examining the effects of a normal pump with a Gaussian carrier distribution and a quiet pump with a sub-Poisson carrier distribution on spectral linewidth and RIN. The results demonstrate a substantial reduction in both spectral linewidth and RIN when using a quiet pump compared to a normal pump, attributed to the lower carrier noise level of the quiet pump. Specifically, at 5.5 times the threshold current, the spectral linewidth decreases from 337.2 kHz to 213.2 kHz, and the RIN decreases from -141.3 dB Hz^{-1} to -168.8 dB Hz^{-1}. Furthermore, with external optical injection locking, the spectral linewidth is further reduced to 24 kHz at an injection ratio of -70 dB, and the RIN also slightly decreases to -172.4 dB Hz^{-1} at an injection ratio of 10. Remarkably, at an injection ratio of 0 dB, the suppression bandwidth reaches 33.6 GHz, achieving an ultra-narrow linewidth of 1.8 mHz, demonstrating excellent linewidth reduction effects. Notably, by reducing external carrier noise, the linewidth rebroadening effect of the QD laser is suppressed, significantly expanding the range of pumping current values under optical injection and enhancing applicability. This provides high-performance light sources for classical optical applications such as optical detection, lidar ranging, and optical communication [28–30], as well as for quantum photonics applications such as quantum computing, continuous-variable quantum key distribution (CV-QKD), and ultra-precise quantum sensing [31–33].

2. Rate equation model of optical-injection-locked QD lasers epitaxially grown on silicon

Figure 1 shows a model of an epitaxial InAs/GaAs QD laser on silicon under optical injection, illustrating two pumping sources with different external carrier noise: a normal pump with a Gaussian carrier distribution and a quiet pump with a sub-Poisson carrier distribution. A tunable laser operates as the master laser for optical injection, while the QD laser serves as the slave laser. The enlarged inset illustrates the electronic

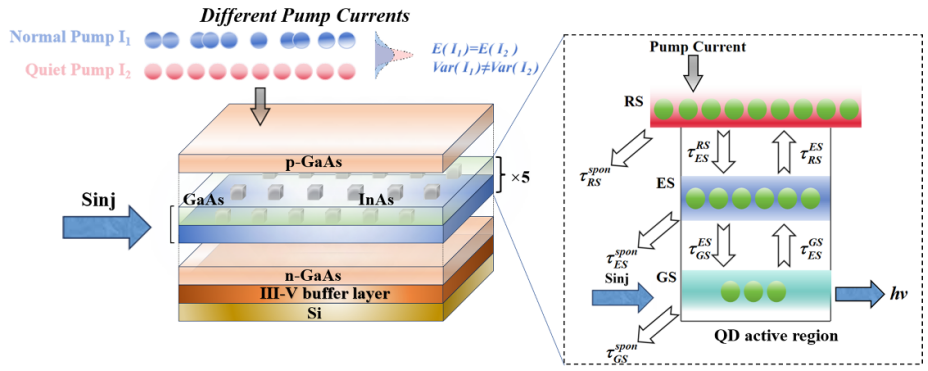

Figure 1. Schematic diagram of the electronic structure and carrier dynamics of a silicon-based QD laser for normal and quiet pumping conditions.

structure of the QD laser and the carrier dynamics in the active region. The numerical model assumes that the active region, which contains a 5-layer QD structure, includes only a single QD ensemble. Therefore, it only considers the effects of homogeneous broadening, while neglecting the inhomogeneous effects caused by QD size distribution. Furthermore, the QDs consistently remain in a neutral state, wherein electrons and holes form electron–hole pairs (excitons) rather than existing independently, resulting in a system composed solely of excitons. The exciton model of the QD laser comprises a two-dimensional carrier reservoir state (RS), a fourfold degenerate excited state (ES), and a twofold degenerate ground state (GS). Upon injection of the pump current, carriers are first captured from the RS to the ES with a capture time of $\tau_{\mathrm{ES}}^{\mathrm{RS}}$, then relax from the ES to the GS with a relaxation time of $\tau_{\mathrm{GS}}^{\mathrm{ES}}$, and finally, stimulated emission occurs in the GS to generate the laser. Due to thermal excitation, carriers can escape from the GS to the ES and from the ES to the RS, with escape times of $\tau_{\mathrm{ES}}^{\mathrm{GS}}$ and $\tau_{\mathrm{RS}}^{\mathrm{ES}}$, respectively. This process is controlled by the Fermi distribution in a quasi-thermal equilibrium state. In addition to stimulated emission, carriers also undergo spontaneous emission, with the spontaneous emission times for each energy state being $\tau_{\mathrm{RS}}^{\mathrm{spon}}$, $\tau_{\mathrm{ES}}^{\mathrm{spon}}$, and $\tau_{\mathrm{GS}}^{\mathrm{spon}}$, respectively. It is noteworthy that, due to the lattice mismatch between silicon and III-V materials, the model includes non-radiative recombination time τ_{SRH} caused by the Shockley–Read–Hall (SRH) process. Therefore, the rate equations describing the carrier numbers N_{RS}, N_{ES}, N_{GS}, the photon number S_{GS}, and the optical field phase ϕ are represented as:

$$\frac{\mathrm{d}N_{\mathrm{RS}}}{\mathrm{d}t} = \frac{\eta I}{q} + \frac{N_{\mathrm{ES}}}{\tau_{\mathrm{RS}}^{\mathrm{ES}}} - \frac{N_{\mathrm{RS}}}{\tau_{\mathrm{ES}}^{\mathrm{RS}}}(1-\rho_{\mathrm{ES}}) - \frac{N_{\mathrm{RS}}}{\tau_{\mathrm{RS}}^{\mathrm{spon}}} - \frac{N_{\mathrm{RS}}}{\tau_{\mathrm{SRH}}} + F_{\mathrm{RS}} \tag{1}$$

$$\frac{\mathrm{d}N_{\mathrm{ES}}}{\mathrm{d}t} = \left(\frac{N_{\mathrm{RS}}}{\tau_{\mathrm{ES}}^{\mathrm{RS}}} + \frac{N_{\mathrm{GS}}}{\tau_{\mathrm{ES}}^{\mathrm{GS}}}\right)(1-\rho_{\mathrm{ES}}) - \frac{N_{\mathrm{ES}}}{\tau_{\mathrm{GS}}^{\mathrm{ES}}}(1-\rho_{\mathrm{GS}}) - \frac{N_{\mathrm{ES}}}{\tau_{\mathrm{RS}}^{\mathrm{ES}}} - \frac{N_{\mathrm{ES}}}{\tau_{\mathrm{ES}}^{\mathrm{spon}}} - \frac{N_{\mathrm{ES}}}{\tau_{\mathrm{SRH}}} + F_{ES} \tag{2}$$

$$\frac{\mathrm{d}N_{\mathrm{GS}}}{\mathrm{d}t} = \frac{N_{\mathrm{ES}}}{\tau_{\mathrm{GS}}^{\mathrm{ES}}}(1-\rho_{\mathrm{GS}}) - \frac{N_{\mathrm{GS}}}{\tau_{\mathrm{ES}}^{\mathrm{GS}}}(1-\rho_{\mathrm{ES}}) - \Gamma_p v_g g_{\mathrm{GS}} S_{\mathrm{GS}} - \frac{N_{\mathrm{GS}}}{\tau_{\mathrm{GS}}^{\mathrm{spon}}} - \frac{N_{\mathrm{GS}}}{\tau_{\mathrm{SRH}}} + F_{\mathrm{GS}} \tag{3}$$

$$\frac{\mathrm{d}S_{\mathrm{GS}}}{\mathrm{d}t} = \left(\Gamma_p v_g g_{\mathrm{GS}} - \frac{1}{\tau_p}\right) S_{\mathrm{GS}} + \beta_{sp}\frac{N_{\mathrm{GS}}}{\tau_{\mathrm{GS}}^{\mathrm{spon}}} + 2k_c\sqrt{S_{\mathrm{inj}}S_{\mathrm{GS}}}\cos\phi + F_S \tag{4}$$

$$\frac{\mathrm{d}\phi}{\mathrm{d}t} = \frac{1}{2}\Gamma_p v_g\left(g_{\mathrm{GS}}\alpha_H^{\mathrm{GS}} + g_{\mathrm{ES}}\alpha_H^{\mathrm{ES}} + g_{\mathrm{RS}}\alpha_H^{\mathrm{RS}}\right) - \Delta\omega_{\mathrm{inj}} - k_c\sqrt{S_{\mathrm{inj}}/S_{\mathrm{GS}}}\sin\phi + F_\phi \tag{5}$$

where η is the injection efficiency, I is the pump current, q is the electron charge, Γ_p is the optical confinement factor, v_g is the group velocity, and β_{sp} is the spontaneous emission factor. The coupling coefficient $k_c = \frac{v_g(1-R)}{2L\sqrt{R}}$ describes the power coupling from one laser cavity to another, where R is the reflectivity of the laser facet, and L is the cavity length of the QD laser. The injection ratio is expressed as $R_{\mathrm{inj}} = \frac{S_{\mathrm{inj}}}{S_0}$, where S_{inj} is the photon number injected from the master laser into the slave laser and S_0 is the steady-state photon number of the free-running slave laser. $\Delta\omega_{\mathrm{inj}}$ is the frequency detuning, representing the frequency difference between the master and slave lasers. g_{RS}, g_{ES}, and g_{GS} are the material gains for each energy state, respectively:

$$g_{\mathrm{RS}} = a_{\mathrm{RS}}\frac{D_{\mathrm{RS}}}{V_{\mathrm{RS}}}(2\rho_{\mathrm{RS}} - 1) \tag{6}$$

$$g_{\mathrm{ES}} = a_{\mathrm{ES}}\frac{N_B}{V_B}(2\rho_{\mathrm{ES}} - 1) \tag{7}$$

$$g_{GS} = \frac{a_{GS}}{1+\epsilon S_{GS}} \frac{N_B}{V_B} (2\rho_{GS} - 1) \tag{8}$$

where the parameters a_{RS}, a_{ES}, and a_{GS} are the differential gains of the material, D_{RS} is the total number of states in the RS, and V_{RS} is the volume of the RS region, N_B is the number of QDs in the active region, V_B is the volume of the active region, ϵ is the gain compression factor. The occupation probabilities of the carriers in each energy state, ρ_{RS}, ρ_{ES}, and ρ_{GS}, are given by $\rho_{RS} = \frac{N_{RS}}{D_{RS}}$, $\rho_{ES} = \frac{N_{ES}}{4N_B}$, and $\rho_{GS} = \frac{N_{GS}}{2N_B}$. The contributions of each energy state to the LEF (α_H), denoted as α_H^{RS}, α_H^{ES}, and α_H^{GS}, are given by the expressions:

$$\alpha_H^{RS} = \frac{\omega_{GS}}{\omega_{RS}} \frac{(\omega_{RS} - \omega_{GS}) T_D}{1 + (\omega_{RS} - \omega_{GS})^2 T_D^2} \tag{9}$$

$$\alpha_H^{ES} = \frac{\omega_{GS}}{\omega_{ES}} \frac{(\omega_{ES} - \omega_{GS}) T_D}{1 + (\omega_{ES} - \omega_{GS})^2 T_D^2} \tag{10}$$

where T_D is the dephasing time, and ω_{RS}, ω_{ES}, and ω_{GS} are the angular frequencies of the respective energy states. Carrier noise and spontaneous emission noise are characterized by Langevin noise sources. F_{RS}, F_{ES}, and F_{GS} represent the carrier noise sources for the RS, ES, and GS states, respectively. F_S and F_ϕ represent the photon noise source and the phase noise source of spontaneous emission, respectively. Both carrier noise and spontaneous emission noise are white noise, and the noise sources are delta-correlated with each other:

$$\langle F_i(t) F_j(t') \rangle = U_{ij} \delta(t - t') \tag{11}$$

where the indexes i and j refer to RS, ES, GS, S, and ϕ. The diffusion coefficients U_{ij} are given by:

$$U_{RSRS} = \frac{\eta I}{q} + \frac{N_{ES}}{\tau_{RS}^{ES}} + \frac{N_{RS}}{\tau_{ES}^{RS}}(1 - \rho_{ES}) + \frac{N_{RS}}{\tau_{RS}^{spon}} + \frac{N_{RS}}{\tau_{SRH}} \tag{12}$$

$$U_{ESES} = 2\left(\frac{N_{RS}}{\tau_{ES}^{RS}} + \frac{N_{GS}}{\tau_{ES}^{GS}}\right)(1 - \rho_{ES}) \tag{13}$$

$$U_{GSGS} = 2\left[\frac{N_{ES}}{\tau_{GS}^{ES}}(1 - \rho_{GS}) - \Gamma_p v_g g_{GS} S_{GS} + \beta_{sp} \frac{N_{GS}}{\tau_{GS}^{spon}} S_{GS}\right] \tag{14}$$

$$U_{SS} = 2S_{GS}\left(\beta_{sp} \frac{N_{GS}}{\tau_{GS}^{spon}} - \Gamma_p v_g g_{GS} + \frac{1}{\tau_p}\right) \tag{15}$$

$$U_{\phi\phi} = \frac{1}{2S_{GS}}\left(\beta_{sp} \frac{N_{GS}}{\tau_{GS}^{spon}} - \Gamma_p v_g g_{GS} + \frac{1}{\tau_p}\right) \tag{16}$$

$$U_{RSES} = -\left[\frac{N_{RS}}{\tau_{ES}^{RS}}(1 - \rho_{ES}) + \frac{N_{ES}}{\tau_{RS}^{ES}}\right] \tag{17}$$

$$U_{ESGS} = -\left[\frac{N_{GS}}{\tau_{ES}^{GS}}(1 - \rho_{ES}) + \frac{N_{ES}}{\tau_{GS}^{ES}}(1 - \rho_{GS})\right] \tag{18}$$

$$U_{GSS} = -\left(2\beta_{sp} \frac{N_{GS}}{\tau_{GS}^{spon}} S_{GS} - \Gamma_p v_g g_{GS} S_{GS}\right) \tag{19}$$

Other unlisted cross-correlation strengths are zeros. Through the small-signal analysis of the rate equations (1)–(5), the linear rate equations in the frequency domain are represented in (20), with the elements of the matrix given in (21).

$$\begin{pmatrix} \gamma_{11} + j\omega & -\gamma_{12} & 0 & 0 & 0 \\ -\gamma_{21} & \gamma_{22} + j\omega & -\gamma_{23} & 0 & 0 \\ 0 & -\gamma_{32} & \gamma_{33} + j\omega & -\gamma_{34} & 0 \\ 0 & 0 & -\gamma_{43} & \gamma_{44} + j\omega & -\gamma_{45} \\ -\gamma_{51} & -\gamma_{52} & -\gamma_{53} & -\gamma_{54} & \gamma_{55} + j\omega \end{pmatrix} \begin{pmatrix} \delta N_{RS} \\ \delta N_{ES} \\ \delta N_{GS} \\ \delta S_{GS} \\ \delta\phi \end{pmatrix} = \begin{pmatrix} F_{RS} \\ F_{ES} \\ F_{GS} \\ F_S \\ F_\phi \end{pmatrix} \tag{20}$$

with

$$\gamma_{11} = \frac{1 - \rho_{ES}}{\tau_{RS}^{ES}} + \frac{1}{\tau_{RS}^{spon}} + \frac{1}{\tau_{SRH}}$$

$$\gamma_{12} = \frac{1}{\tau_{RS}^{ES}} + \frac{1}{4N_B} \frac{N_{RS}}{\tau_{ES}^{RS}}, \gamma_{21} = \frac{1 - \rho_{ES}}{\tau_{RS}^{ES}}$$

$$\gamma_{22} = \frac{1-\rho_{GS}}{\tau_{GS}^{ES}} + \frac{1}{\tau_{RS}^{ES}} + \frac{1}{\tau_{ES}^{spon}} + \frac{1}{4N_B}\left(\frac{N_{RS}}{\tau_{ES}^{RS}} + \frac{N_{GS}}{\tau_{ES}^{GS}}\right) + \frac{1}{\tau_{SRH}}$$
$$\gamma_{23} = \frac{1-\rho_{ES}}{\tau_{ES}^{GS}} + \frac{1}{2N_B}\frac{N_{ES}}{\tau_{GS}^{ES}}$$
$$\gamma_{32} = \frac{1-\rho_{GS}}{\tau_{GS}^{ES}} + \frac{1}{4N_B}\frac{N_{GS}}{\tau_{ES}^{GS}}$$
$$\gamma_{33} = \frac{1-\rho_{ES}}{\tau_{ES}^{GS}} + \frac{1}{2N_B}\frac{N_{ES}}{\tau_{GS}^{ES}} + \frac{1}{\tau_{GS}^{spon}} + \frac{1}{\tau_{SRH}} + \Gamma_p v_g a S_{GS}$$
$$\gamma_{34} = -\Gamma_p v_g g_{GS} + \Gamma_p v_g a_p S_{GS}$$
$$\gamma_{43} = \Gamma_p v_g a S_{GS} + \frac{\beta_{sp}}{\tau_{GS}^{spon}}$$
$$\gamma_{44} = \frac{1}{\tau_p} - \Gamma_p v_g g_{GS} + \Gamma_p v_g a_p S_{GS} - k_c \cos\phi \sqrt{S_{inj}/S_{GS}}$$
$$\gamma_{45} = -2k_c \sin\phi \sqrt{S_{inj} S_{GS}}, \gamma_{51} = \Gamma_p v_g a_{RS} \alpha_H^{RS}$$
$$\gamma_{52} = \frac{1}{4}\Gamma_p v_g a_{ES} \alpha_H^{ES}, \gamma_{53} = \frac{1}{2}\Gamma_p v_g a \alpha_H^{GS}$$
$$\gamma_{54} = -\frac{1}{2}\Gamma_p v_g a_p \alpha_H^{GS} + \frac{k_c}{2S_{GS}} \sin\phi \sqrt{S_{inj}/S_{GS}}$$
$$\gamma_{55} = k_c \cos\phi \sqrt{S_{inj}/S_{GS}} \tag{21}$$

In small-signal analysis, the gain compression effect is represented by a_p and can be expressed as $\delta g_{GS} = a\delta N_{GS} - a_p \delta S_{GS}$. Using Cramer's rule, the small-signal variations in photon number δS_{GS} and phase $\delta\phi$ can be determined. The RIN and FN can be expressed as:

$$\mathrm{RIN}(\omega) = \left|\frac{\delta S_{GS}(\omega)}{S_{GS}}\right|^2 \tag{22}$$
$$\mathrm{FN}(\omega) = \left|\frac{j\omega}{2\pi}\delta\phi(\omega)\right|^2 \tag{23}$$

where S_{GS} is the number of photons during the stable operation of the laser, and ω is the angular frequency. The Schawlow–Townes linewidth $\Delta\nu_{ST}$ of the QD laser can be extracted from the high-frequency part of the FN spectrum as $\Delta\nu_{ST} = 2\pi FN|_{f=100\,\mathrm{GHz}}$, while the spectral linewidth $\Delta\nu_{OL}$ can be extracted from the low-frequency part of the FN spectrum as $\Delta\nu_{OL} = 2\pi FN|_{f=1\,\mathrm{MHz}}$. The spectral linewidth of the QD laser is broadened beyond the Schawlow–Townes linewidth by a factor of α_H, and can be expressed as:

$$\Delta\nu_{OL} = \Delta\nu_{ST}\left(1+\alpha_H^2\right) \tag{24}$$

where $\Delta\nu_{ST}$ is determined solely by spontaneous emission, while $\Delta\nu_{OL}$ depends not only on spontaneous emission but also on the additional carrier fluctuations induced by α_H. To facilitate a comparative analysis of the impact of different external carrier noise on laser performance, the QW model, as referenced in [34], is also examined. Table 1 lists all material and optical parameters used in the simulation. The free-running QD laser in the model exhibits a threshold current of $I_{th} = 55\,\mathrm{mA}$. When pumped at 5.5 times this threshold current, the photon number in the laser cavity reaches 6.9×10^5. The steady state of the QD laser is derived from the time-integrated sequence of photon numbers.

3. Results and discussion

The related diffusion coefficient U_{RSRS} is a key parameter linking the optical noise of laser and external carrier noise. When the QD laser is driven by a normal pump, a noise term $\frac{\eta I}{q}$ is added to the U_{RSRS} term to account for the impact of external carrier noise on the active region of the QD laser. Conversely, when the QD laser is driven by a quiet pump, the noise term $\frac{\eta I}{q}$ is removed from the U_{RSRS} term, assuming that external carrier noise has no effect on the laser. Based on the above assumption, the FN spectra and spectral linewidths of both QD lasers and QW lasers are obtained. Figure 2 illustrates the FN and spectral linewidth of silicon-based QD and QW lasers operating at 5.5 times the threshold current. In figure 2(a), it is evident that the FN of QD lasers displays a noticeable resonance peak around the relaxation oscillation frequency (ROF), which is approximately 7 GHz. Above this resonance peak, the FN stabilizes at a constant level, whereas below the peak, external carrier noise significantly impacts the FN. Notably, silicon-based QD lasers

Table 1. Material and optical parameters of the QD laser.

Symbol	Description	Value
E_{RS}	RS energy level	1.19 eV
E_{ES}	ES energy level	1.03 eV
E_{GS}	GS energy level	0.95 eV
τ_{ES}^{RS}	RS to ES capture time	6.3 ps
τ_{GS}^{ES}	ES to GS relaxation time	2.9 ps
τ_{RS}^{ES}	ES to RS escape time	29.6 ns
τ_{ES}^{GS}	GS to ES escape time	34.5 ps
τ_{RS}^{spon}	RS spontaneous emission lifetime	0.5 ns
τ_{ES}^{spon}	ES spontaneous emission lifetime	0.5 ns
τ_{GS}^{spon}	GS spontaneous emission lifetime	1.2 ns
τ_p	Photon lifetime	4.1 ps
T_D	Polarization dephasing time	0.1 ps
τ_{SRH}	Nonradiative recombination lifetime	1 ns
β_{sp}	Spontaneous emission factor	1.0×10^{-4}
ϵ	Gain compression factor	2.0×10^{-16} cm^3
Γ_p	Optical confinement factor	0.06
a_{GS}	GS Differential gain	5.0×10^{-15} cm^2
a_{ES}	ES Differential gain	1.0×10^{-15} cm^2
a_{RS}	RS Differential gain	2.5×10^{-15} cm^2
α_{GS}^{H}	GS contribution to α_H-factor	0.50
N_B	Total dot number	1.0×10^7
D_{RS}	Total RS state number	4.8×10^6
V_B	The volume of active region	5.0×10^{-11} cm^3
V_{RS}	The volume of RS region	1.0×10^{-11} cm^3
k_c	Injection coupling coefficient	10×10^{10}s^{-1}

using the quiet pump exhibit a lower FN compared to those using the normal pump. Figure 2(b) shows that QW lasers have a resonance peak around 32 GHz, indicating a much higher ROF and superior modulation characteristics compared to QD lasers. However, the peak amplitude of QD lasers is significantly lower than that of QW lasers, suggesting a larger damping factor in QD lasers, which is advantageous for low-noise applications [14]. Additionally, in QW lasers, the FN of the two pumping sources nearly coincides at frequencies below the resonance peak, suggesting that external carrier noise has minimal effect on the low-frequency FN. However, for QD lasers, simulations confirm that carrier noise significantly impacts the overall FN of the laser. To further illustrate this, figure 2 demonstrates that when all external carrier noise, including noise from the RS, ES, GS, and noise from the pump current, is eliminated (as depicted by the red dashed line), the FN slightly decreases compared to lasers using the quiet pump. Using equation (17), the spectral linewidths as a function of normalized bias current for QD lasers and QW lasers are extracted from the FN spectrum to further illustrate the impact of external carrier noise on these lasers. As shown in figure 2(c), the spectral linewidth of the QD laser is significantly narrower under the quiet pump compared to the normal pump. The difference in linewidth between the two pumping conditions becomes more pronounced with increasing pumping current due to the linewidth rebroadening effect occurring at high currents under normal pumping conditions. In addition to the spectral linewidth rebroadening phenomenon shown in figure 2(c), QD lasers at high pump level can also encounter issues such as reduced quantum efficiency, degradation of optical quality, rollover of $I-V$ characteristics [35], and catastrophic facet degradation at the highest power levels, which are more obvious in the silicon-based QD lasers [36]. Although the semi-classical rate equation model employed in this paper does not account for these factors, the qualitative conclusions drawn from the subsequent simulations remain unchanged. At 5.5 times the threshold current, the spectral linewidth of the QD laser under the normal pump is 337.2 kHz, while it is reduced to 213.2 kHz under the quiet pump. This behavior is attributed to the increase in external carrier noise at high currents under normal pumping conditions. Notably, the quiet pump also suppresses the effect of spectral linewidth rebroadening. Even at high pumping currents, specifically at 10 times the threshold current, the spectral linewidth continues to decrease with increasing bias current, and the spectral linewidth of the QD laser under the quiet pump is 131 kHz, which is only a quarter of that under the normal pump. The inset in figure 2(c) further elucidates the different behaviors of the spectral linewidth under the two pumping conditions. As the pumping current increases, the influence of carriers in the ES on the GS becomes more significant under the normal pump, causing an increase in α_H and consequently an increase in spectral linewidth. Quiet pump suppresses the influence of carriers in the ES on the GS, resulting in α_H

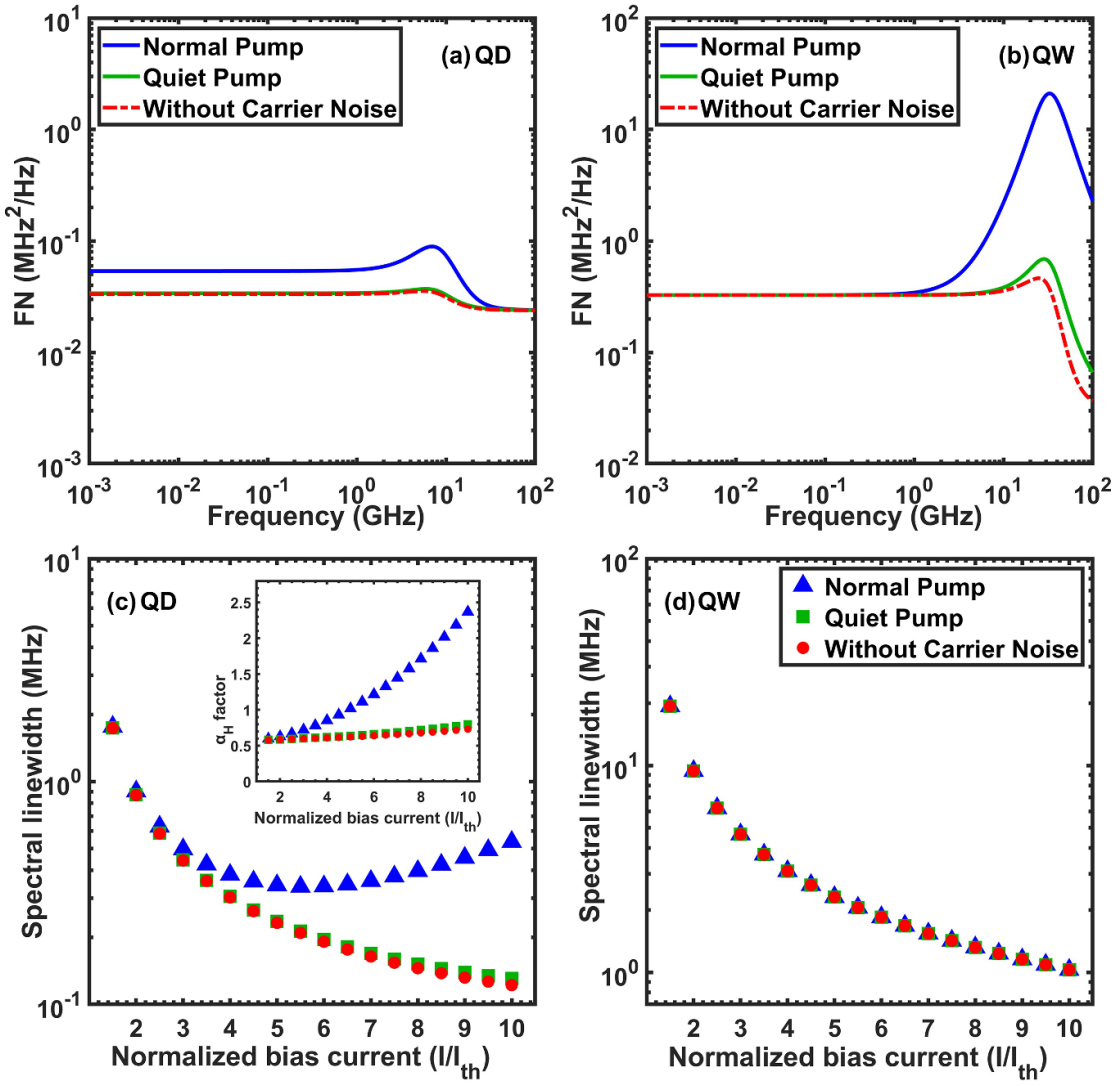

Figure 2. FN spectrum of (a) epitaxial QD laser on silicon and (b) silicon-based QW laser under normal and quiet pumping conditions. The spectral linewidth as a function of normalized bias current for (c) epitaxial QD lasers on silicon and (d) silicon-based QW lasers under normal pump and quiet pump. The inset of (c) shows the dependence of α_H on the bias current of the QD laser.

remaining almost unchanged with increasing pumping current, thereby preventing spectral linewidth rebroadening. Figure 2(d) demonstrates that the different external carrier noises associated with various pumping sources have almost no effect on the linewidth of the QW laser [37]. In practical applications, the choice of pumping source does not significantly affect the optical noise properties of the QW laser.

The above results illustrate that for QD lasers, using quiet pump with low external carrier noise is crucial, as the reduction in carrier noise significantly improves laser noise performance. The impact of external carrier noise on the RIN of QD lasers is also examined. Figure 3(a) compares the RIN spectra at 5.5 times the threshold current under normal and quiet pumping conditions. When quiet pump is employed, the low-frequency RIN value notably decreases from -141.3 dB Hz^{-1} to -168.8 dB Hz^{-1}, compared to normal pump where the laser exhibits overdamping. It can also be observed that the laser exhibits under-damping, and the peak amplitude of the QD laser using the quiet pump is significantly higher than that of the laser using the normal pump. This observation indicates that the quiet pump enhances the modulation efficiency of the laser, which is beneficial for high-speed communication applications. Figure 3(b) presents the low-frequency RIN of QD lasers under the normal and the quiet pump as a function of normalized bias current. It shows that, for both pumping conditions, the RIN decreases with increasing pumping current. However, the RIN under quiet pump remains consistently around 30 dB lower than under normal pump. This reduction in RIN demonstrates that the quiet pump mitigates the adverse effects of external carrier noise, leading to improved laser performance and reduced noise levels. Consequently, quiet pumping sources

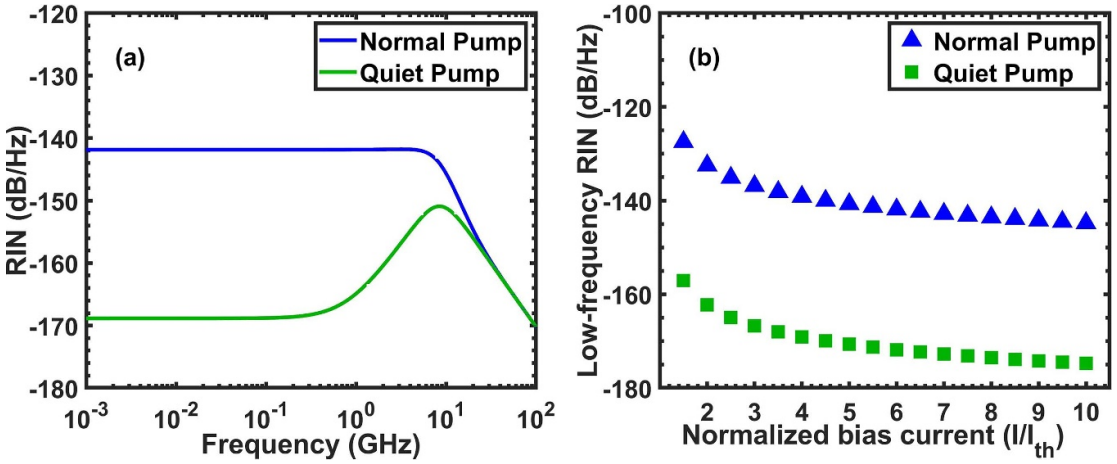

Figure 3. (a) RIN spectrum of epitaxial QD lasers on silicon under normal pump and quiet pump. (b) Low-frequency RIN of epitaxial QD lasers on silicon versus normalized bias current under normal pump and quiet pump.

prove to be stable and reliable in lowering the RIN of QD lasers, effectively reducing output power fluctuations.

The impact of external carrier noise on silicon-based QD lasers under optical injection locking is now being investigated. Figure 4(a) illustrates the FN spectrum of the QD laser at various injection ratios and zero frequency detuning with a quiet pump set at 5.5 times the threshold current. This specific current level is selected for optical injection locking because, as demonstrated in figure 2(c), the QD laser achieves its minimum linewidth before the linewidth rebroadening at 5.5 times the threshold current under normal pump conditions. The goal is to further reduce the optical noise of the laser through this method. Due to the strong low-frequency phase locking between the master laser and the slave laser, the FN at low frequencies significantly decreases with increasing injection ratio. Figure 4(b) shows the spectral linewidth extracted from the FN at 1 MHz as a function of the injection ratio under both normal pump and quiet pump conditions. Compared to normal pump, the spectral linewidth of lasers using quiet pump is slightly narrower at all injection ratios. Under quiet pump, the spectral linewidth sharply decreases from 213.2 kHz to 24.3 kHz at a low injection ratio of −70 dB. An ultra-narrow linewidth of 1.8 mHz is achieved at an injection ratio of 0 dB. Notably, the spectral linewidth of the optical-injection-locked QD laser is controlled solely by the FN of the master laser and no longer follows the Schawlow–Townes limit of the free-running laser. To measure the low-frequency range of phase locking between the master and slave lasers, the suppression bandwidth is defined. Within this bandwidth, the FN is reduced by −3 dB compared to the FN of the free-running QD laser. Consequently, the FN below the suppression bandwidth is primarily determined by the master laser, while the FN above the suppression bandwidth is predominantly influenced by the slave laser [22]. Figures 4(c) and (d) provide a mapping of the suppression bandwidth as a function of injection ratio and frequency detuning under normal and quiet pumping conditions. The results show that, for both pumping conditions, the suppression bandwidth increases with the injection ratio at a given frequency detuning, reaching its maximum at zero frequency detuning. Under normal pump, the maximum suppression bandwidth is 14.1 GHz, while under quiet pump, it reaches 33.6 GHz. By comparing figures 4(c) and (d), it is evident that within the injection space defined by the injection ratio and frequency detuning, the QD laser under the quiet pump has a larger stability area and a greater suppression bandwidth. This indicates that using a quiet pump significantly enhances the performance of the epitaxial QD laser on silicon under optical injection locking. From a practical application perspective, although optical injection is an excellent method for suppressing spectral linewidth, it requires a high-quality master laser with a narrow linewidth. Figures 4(c) and (d) show that by improving the quality of the pump source, the requirements on the master laser can be reduced, thereby enhancing the effectiveness of optical injection.

It has been found that a very low injection ratio can significantly reduce the spectral linewidth of the laser. Consequently, the injection ratio is typically expressed in decibels (dB) when describing the FN of QD lasers. However, in this section, the injection ratio is converted back to a dimensionless value when describing the RIN. Figure 5(a) shows the RIN spectrum of a silicon-based QD laser using the quiet pump at 5.5 times the threshold current under different injection ratios and zero frequency detuning. As the injection

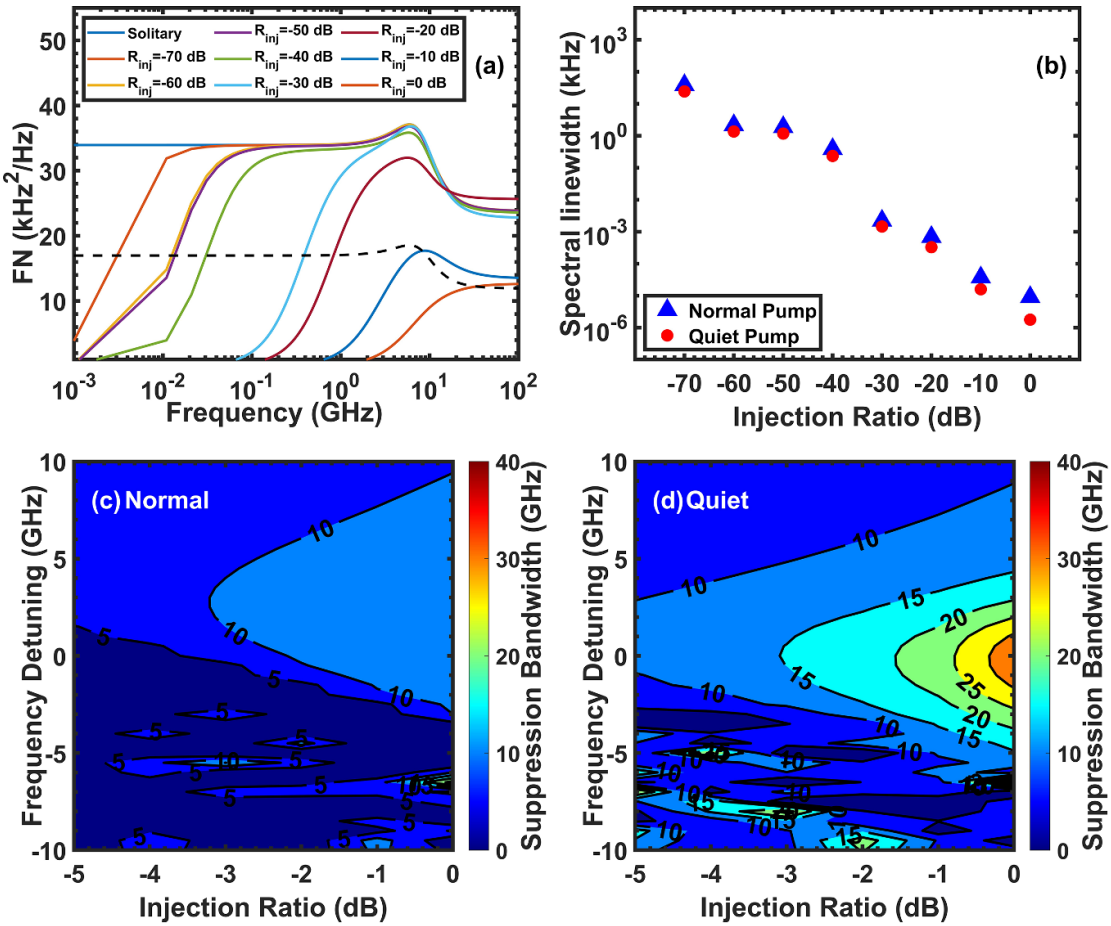

Figure 4. (a) FN spectra at different injection ratios and zero frequency detuning under quiet pump. The black dashed line indicates −3 dB of the FN of the solitary laser. (b) Spectral linewidth at different injection ratios for different pumping conditions. Suppression bandwidth with the variation of injection ratio and frequency detuning under (c) normal pump and (d) quiet pump.

ratio increases, the RIN decreases across the entire frequency range, with the resonance peak frequency shifting higher and the peak RIN amplitude decreasing. This occurs because the number of photons in the steady state increases with the injection ratio, leading to an increase in the damping factor [17]. Since the modulation characteristics and the RIN spectrum of the QD laser are governed by the same dynamic processes within the laser [38], figure 5(a) also demonstrates that the modulation characteristics of the laser improve with increasing injection ratios. Figure 5(b) shows the variation of low-frequency RIN at 1 MHz for different injection ratios under various pumping conditions. As the injection ratio increases, the low-frequency RIN values of QD lasers decrease, regardless of the pumping source used. Under normal pump, the low-frequency RIN value decreases from −145.2 dB Hz^{-1} at an injection ratio of 1 to −150.4 dB Hz^{-1} at an injection ratio of 10. In contrast, under quiet pump, the low-frequency RIN value decreases slightly from −169.5 dB Hz^{-1} at an injection ratio of 1 to −171.9 dB Hz^{-1} at an injection ratio of 10. Notably, the low-frequency RIN value under quiet pump is consistently about 20 dB lower than that under normal pump. Notably, similar to the FN, the RIN of the QD laser, when injection-locked, is also dominated by the master laser [22]. Figures 5(c) and (d) respectively show the mapping of low-frequency RIN variations with injection ratio and frequency detuning under normal and quiet pumping conditions. It is evident that the RIN of the QD laser using a quiet pump is lower across the entire injection space defined by frequency detuning and injection ratio. At the maximum injection ratio of 10, the RIN of the laser under quiet pumping reaches −172.4 dB Hz^{-1}, which is approximately 10 dB lower than that under normal pump. Additionally, outside the stable locked area, the negative detuning area is more chaotic than the positive detuning area, due to the smaller α_H factor at shorter wavelengths compared to longer wavelengths [39, 40].

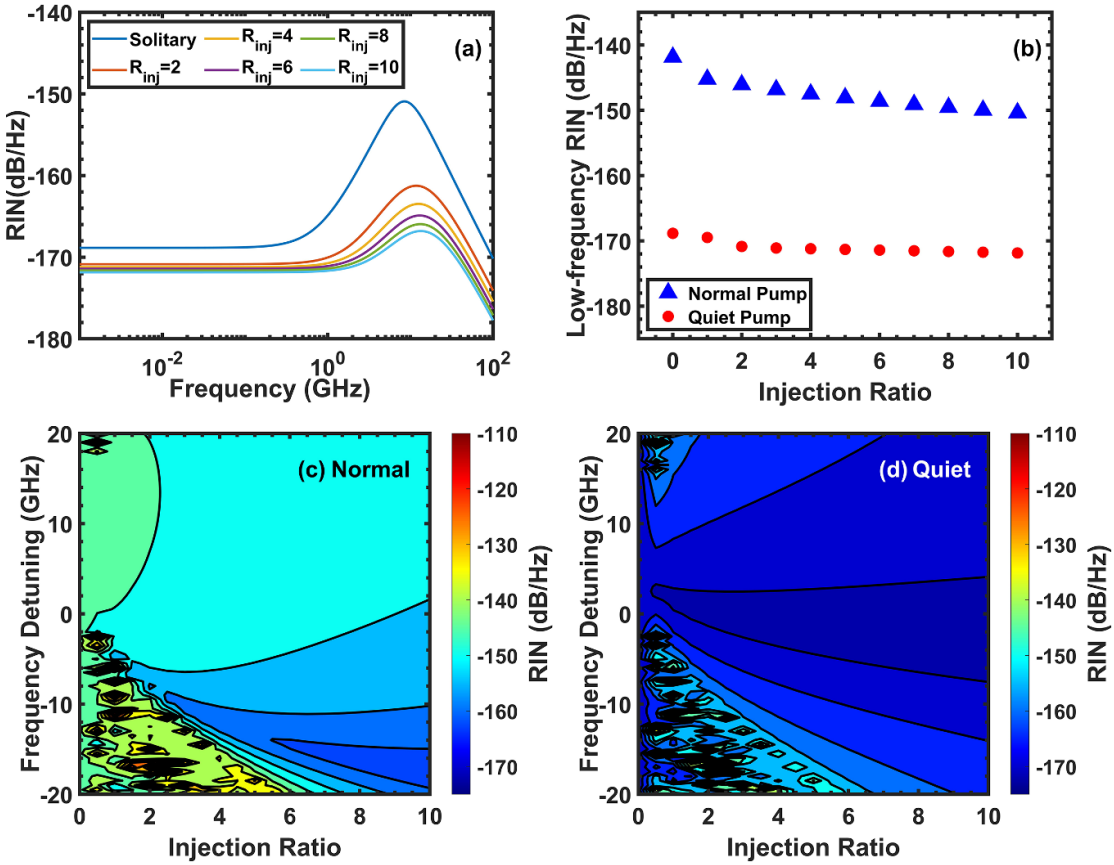

Figure 5. (a) RIN spectra at different injection ratios and zero frequency detuning under quiet pump. (b) Low-frequency RIN at different injection ratios and zero frequency detuning for different pumping conditions. Low-frequency RIN with the variation of injection ratio and frequency detuning under (c) normal pump and (d) quiet pump.

4. Conclusions

This paper theoretically investigates the impact of reducing external carrier noise from the pumping source on epitaxial QD lasers on silicon under optical injection locking. The presence of external carrier noise increases the optical noise and reduces the stability of the lasers. These results indicate that by using the quiet pump, the spectral linewidth and RIN of QD lasers can be effectively reduced, and the suppression bandwidth can be increased. Through quiet pump, an ultra-narrow linewidth of 1.8 mHz and a suppression bandwidth of 33.6 GHz can be achieved at an injection ratio of 0 dB. Additionally, quiet pump can achieve a RIN as low as -172.4 dB Hz^{-1} at an injection ratio of 10, which is a reduction of 10 dB compared to normal pump at the same injection ratio. This improvement is beneficial for achieving amplitude-squeezed states and can serve as a light source for quantum communication. Quiet pump has an optimization on the LEF and RIN of QD comb lasers [41], and the linewidth of QD lasers can also be reduced by using quiet pumping [26], as the existing experimental results are consistent with the conclusions that have been obtained in this study. Consequently, quiet pump provides an effective and simple method for advancing quantum communication systems based on QD lasers [42]. Overall, this work demonstrates epitaxial QD lasers on silicon with extremely narrow linewidths and very low RIN, making them suitable for a wide range of applications, including coherent detection, radar monitoring, optical communication, and cutting-edge quantum photonics applications such as CV-QKD and quantum computing.

Data availability statement

The data cannot be made publicly available upon publication because no suitable repository exists for hosting data in this field of study. The data that support the findings of this study are available upon reasonable request from the authors.

Acknowledgments

Authors acknowledge Prof. Frédéric Grillot and Dr Shiyuan Zhao from Telecom Paris, Institut Polytechnique de Paris, for their fruitful discussions.

Funding

This work was supported by the National Key Research and Development Program of China (2022YFB2803600), the National Natural Science Foundation of China (62204072, U22A2093, 62334013), the Basic and Applied Basic Research Foundation of Guangdong Province (2021A1515110076, 2023A1515012304, 2023A1515011944), the Shenzhen Science and Technology Innovation Program (GXWD20220811163623002, RCBS20210609103824050, JCYJ20220531095604009, RCYX20221008092907027), and the Fundamental Research Funds for the Central Universities (HIT.DZJJ.2023115).

ORCID iDs

Qi Chu https://orcid.org/0009-0006-6328-1841
Shihao Ding https://orcid.org/0000-0003-4641-6944
Jianan Duan https://orcid.org/0000-0001-7710-4287

References

[1] Zhou Z, Ou X, Fang Y, Alkhazraji E, Xu R, Wan Y and Bowers J E 2023 Prospects and applications of on-chip lasers *Elight* **3** 1
[2] Xiang C *et al* 2021 High-performance silicon photonics using heterogeneous integration *IEEE J. Sel. Top. Quantum Electron.* **28** 1–15
[3] Xiang C, Bowers S M, Bjorlin A, Blum R and Bowers J E 2021 Perspective on the future of silicon photonics and electronics *Appl. Phys. Lett.* **118** 22
[4] Gomez S, Huang H, Duan J, Combrié S, Shen A, Baili G, de Rossi A and Grillot F 2020 High coherence collapse of a hybrid III–V/Si semiconductor laser with a large quality factor *J. Phys. Photon.* **2** 025005
[5] Hussin R J and Karomi I B 2024 Progressing in III-V semiconductor quantum dot lasers grown directly on silicon: a review *Silicon* **16** 1–14
[6] Zhao S and Grillot F 2021 Effect of shockley-read-hall recombination on the static and dynamical characteristics of epitaxial quantum-dot lasers on silicon *Phys. Rev.* A **103** 063521
[7] Moody G *et al* 2022 Roadmap on integrated quantum photonics *J. Phys. Photon.* **4** 012501
[8] Beanland R, Sánchez A M, Childs D, Groom K M, Liu H Y, Mowbray D J and Hopkinson M 2008 Structural analysis of life tested 1.3 μm quantum dot lasers *J. Appl. Phys.* **103** 014913
[9] Liu J, Tang M, Deng H, Shutts S, Wang L, Smowton P M, Jin C, Chen S, Seeds A and Liu H 2022 Theoretical analysis and modelling of degradation for III–V lasers on Si *J. Phys. D: Appl. Phys.* **55** 404006
[10] Norman J C, Jung D, Zhang Z, Wan Y, Liu S, Shang C, Herrick R W, Chow W W, Gossard A C and Bowers J E 2019 A review of high-performance quantum dot lasers on silicon *IEEE J. Quantum Electron.* **55** 1–11
[11] Nishi K, Takemasa K, Sugawara M and Arakawa Y 2017 Development of quantum dot lasers for data-com and silicon photonics applications *IEEE J. Sel. Top. Quantum Electron.* **23** 1–7
[12] Duan J, Huang H, Dong B, Norman J C, Zhang Z, Bowers J E and Grillot F 2019 Dynamic and nonlinear properties of epitaxial quantum dot lasers on silicon for isolator-free integration *Photon. Res.* **7** 1222–8
[13] XTDong B, de Labriolle X C, Liu S, Dumont M, Huang H, Duan J, Norman J C, Bowers J E and Grillot F 2020 1.3-μm passively mode-locked quantum dot lasers epitaxially grown on silicon: gain properties and optical feedback stabilization *J. Phys. Photon.* **2** 045006
[14] Duan J, Huang H, Lu Z G, Poole P J, Wang C and Grillot F 2018 Narrow spectral linewidth in InAs/InP quantum dot distributed feedback lasers *Appl. Phys. Lett.* **112** 121102
[15] Norman J C, Jung D, Wan Y and Bowers J E 2018 Perspective: the future of quantum dot photonic integrated circuits *APL Photon.* **3** 030901
[16] Duan J, Huang H, Dong B, Jung D, Norman J C, Bowers J E and Grillot F 2019 1.3-μm reflection insensitive InAs/GaAs quantum dot lasers directly grown on silicon *IEEE Photonics Technol. Lett.* **31** 345–8
[17] Chu Q, Zhao S, Wang J, Sun Y, Yao Y, Xu X, Grillot F and Duan J 2023 Optical noise characteristics of injection-locked epitaxial quantum dot lasers on silicon *Opt. Express* **31** 25177–90
[18] Erneux T, Viktorov E A, Kelleher B, Goulding D, Hegarty S P and Huyet G 2010 Optically injected quantum-dot lasers *Opt. Lett.* **35** 937–9
[19] Wang C, Chaibi M E, Huang H, Erasme D, Poole P, Even J and Grillot F 2015 Frequency-dependent linewidth enhancement factor of optical injection-locked quantum dot/dash lasers *Opt. Express* **23** 21761–70
[20] Wang C, Raghunathan R, Schires K, Chan S-C, Lester L F and Grillot F 2016 Optically injected InAs/GaAs quantum dot laser for tunable photonic microwave generation *Opt. Lett.* **41** 1153–6
[21] Jiang Z-F, Wu Z-M, Jayaprasath E, Yang W-Y, Hu C-X and Xia G-Q 2019 Nonlinear dynamics of exclusive excited-state emission quantum dot lasers under optical injection *Photonics* **6** 58
[22] Wang X-G, Zhao B-B, Grillot F and Wang C 2018 Frequency noise suppression of optical injection-locked quantum cascade lasers *Opt. Express* **26** 15167–76
[23] Redlich C, Lingnau B, Huang H, Raghunathan R, Schires K, Poole P, Grillot F and Lüdge K 2017 Linewidth rebroadening in quantum dot semiconductor lasers *IEEE J. Sel. Top. Quantum Electron.* **23** 1–10

[24] Köster F, Duan J, Dong B, Huang H, Grillot F and Lüdge K 2020 Temperature dependent linewidth rebroadening in quantum dot semiconductor lasers *J. Phys. D: Appl. Phys.* **53** 235106
[25] Zhao S and Grillot F 2022 Stochastic model of sub-poissonian quantum light in an interband cascade laser *Phys. Rev. Appl.* **18** 064027
[26] Ding S, Zhao S, Huang H and Grillot F 2023 Impact of external carrier noise on the linewidth enhancement factor of a quantum dot distributed feedback laser *Opt. Express* **31** 35343–53
[27] Mork J and Yvind K 2020 Squeezing of intensity noise in nanolasers and nanoLEDs with extreme dielectric confinement *Optica* **7** 1641–4
[28] Martin A *et al* 2018 Photonic integrated circuit-based FMCW coherent LiDAR *J. Lightwave Technol.* **36** 4640–5
[29] Xiang C *et al* 2021 High-performance lasers for fully integrated silicon nitride photonics *Nat. Commun.* **12** 6650
[30] Liu S, Wu X, Jung D, Norman J C, Kennedy M J, Tsang H K, Gossard A C and Bowers J E 2019 High-channel-count 20 GHz passively mode-locked quantum dot laser directly grown on Si with 4.1 Tbit/s transmission capacity *Optica* **6** 128–34
[31] Scarani V, Bechmann-Pasquinucci H, Cerf N J, Dušek M, Lütkenhaus N and Peev M 2009 The security of practical quantum key distribution *Rev. Mod. Phys.* **81** 1301–50
[32] Kok P, Munro W J, Nemoto K, Ralph T C, Dowling J P and Milburn G J 2007 Linear optical quantum computing with photonic qubits *Rev. Mod. Phys.* **79** 135–74
[33] Barsotti L, Harms J and Schnabel R 2018 Squeezed vacuum states of light for gravitational wave detectors *Rep. Prog. Phys.* **82** 016905
[34] Coldren L A, Corzine S W and Mashanovitch M L 2012 *Diode Lasers and Photonic Integrated Circuits* vol 218 (Wiley)
[35] Liu A Y, Zhang C, Norman J, Snyder A, Lubyshev D, Fastenau J M, Liu A W K, Gossard A C and Bowers J E 2014 High performance continuous wave 1.3 μm quantum dot lasers on silicon *Appl. Phys. Lett.* **104** 041104
[36] Liu A Y *et al* 2015 Quantum dot lasers for silicon photonics [Invited] *Photon. Res.* **3** 050000B1
[37] Duan J, Wang X-G, Zhou Y-G, Wang C and Grillot F 2018 Carrier-noise-enhanced relative intensity noise of quantum dot lasers *IEEE J. Quantum Electron.* **54** 1–7
[38] Duan J, Zhou Y, Dong B, Huang H, Norman J C, Jung D, Zhang Z, Wang C, Bowers J E and Grillot F 2020 Effect of p-doping on the intensity noise of epitaxial quantum dot lasers on silicon *Opt. Lett.* **45** 4887–90
[39] Duan J, Huang H, Jung D, Zhang Z, Norman J, Bowers J E and Grillot F 2018 Semiconductor quantum dot lasers epitaxially grown on silicon with low linewidth enhancement factor *Appl. Phys. Lett.* **112** 251111
[40] Li N, Susanto H, Cemlyn B R, Henning I D and Adams M J 2018 Nonlinear dynamics of solitary and optically injected two-element laser arrays with four different waveguide structures: a numerical study *Opt. Express* **26** 4751–65
[41] Wang W *et al* 2024 Intensity noise reduction in quantum dot comb laser by lower external carrier fluctuations *Opt. Lett.* **49** 5007–10
[42] Ding S, Zhao S, Huang H and Grillot F 2024 Observation of amplitude squeezing in a constant-current-driven distributed feedback quantum dot laser with optical feedback *APL Quantum* **1** 026104